SCATTERING OF REAL AND VIRTUAL PHOTONS AT HERA*

M.W. KRASNY

L.P.N.H.E, IN2P3-CNRS, Universities Paris VI et VII
4, pl. Jussieu, T33 RdC, 75252 Paris Cedex 05, France

(Received March 27, 1996)

In this note I discuss recent results obtained by the two experiments H1 and ZEUS at the first electron proton collider — HERA. In particular, I concentrate on results which are of importance for our understanding of the nature of strong interactions. In the weak coupling limit of strong interactions *i.e.* in the processes involving short distances, perturbative Quantum Chromodynamics can be confronted with the HERA data in a new regime. What is however more challenging is the unique possibility of HERA to map the transition from the regime of the short distance phenomena, which are controlled by perturbative QCD, to the large distance phenomena where perturbative QCD can not be applied.

PACS numbers: 12.38.Aw, 12.38.Qk

1. Introduction

The *ep* collider HERA, in which 27.6 GeV electrons collide with 820 GeV protons, opens several new research domains. The two colliding beam experiments H1 and ZEUS have been taking and analyzing the electron-proton scattering data at energies up to $\sqrt{s} = 300$ GeV since 1992. In 1995 the HERMES experiment became operational and is presently investigating the scattering of polarized electrons on polarized stationary targets of helium, deuterium and hydrogen. The HERA-B experiment has been approved recently to measure the CP-violating decays of B-mesons produced by HERA protons scattered off a stationary tungsten target. The future program at HERA which is presently being discussed includes the scattering of electrons on nuclei, both in the fixed target mode and in the colliding

* Presented at the Cracow Epiphany Conference on Proton Structure, Kraków, Poland, January 5–6, 1996.

mode as well as a possible program of scattering of polarized electrons on polarized protons in the colliding mode.

Two kinematical variables x and Q^2 specify the kinematics of electron-proton scattering at fixed CM energy $\sqrt{s}$. They can be calculated from four-momenta of the incoming electron, k, of the scattered electron, k', and incoming proton P as:

$$Q^2 = -(k' - k)^2 , \tag{1}$$

$$x = \frac{Q^2}{2P(k' - k)} . \tag{2}$$

The momentum transferred squared, Q^2, defines the resolution power of the virtual boson exchanged between the electron and the proton in the plane transverse to their momenta. The photon of virtuality Q^2 resolves the structure of the target at distances of $d \approx 1/\sqrt{Q^2}$. The Bjorken variable x has a very simple interpretation in the reference system in which the proton moves with large momentum (infinite momentum frame). It can be interpreted [1] as the momentum fraction of the proton carried by a charged parton on which the electron scatters elastically. This interpretation is valid in the Bjorken limit [2] for Q^2 values much larger than a typical scale of the hadronic masses. In addition the variable x can be related [3] to the longitudinal localization of the interaction volume where the electron couples to the charged parton, $l \approx 1/x$.

At HERA, owing to large $\sqrt{s}$ and the wide angular acceptance of both H1 [4] and ZEUS [5] detectors, the electron-proton scattering processes can be studied in a vast range of x and Q^2 variables, extending over 10 orders of magnitude. This unique feature of the HERA experiments enables us to study both the photo-production processes ($Q^2 = 10^{-5} - 10^{-2}$ GeV^2) and the deep inelastic scattering (DIS) processes, where the resolution power of the virtual photon reaches the distances of 10^{-17} m. In the DIS regime of electron-proton scattering ($Q^2 \geq 2$ GeV^2) HERA experiments cover four orders of magnitude in x and, as shown in Fig. 1, extend significantly the measurement domain of the previous DIS experiments.

For the first time the domain of low x in DIS regime can be explored, where the longitudinal localization of the interaction volume is 1000 times larger than the size of the proton. HERA can thus be considered as a dedicated machine for exploring the transition region between the short distance and long distance strong interactions and for verifying the validity of perturbative QCD in this transition region.

Several important experimental results have been obtained from the analysis of the data collected over the first three years of HERA operation. For these lectures I selected predominantly those corresponding to the DIS

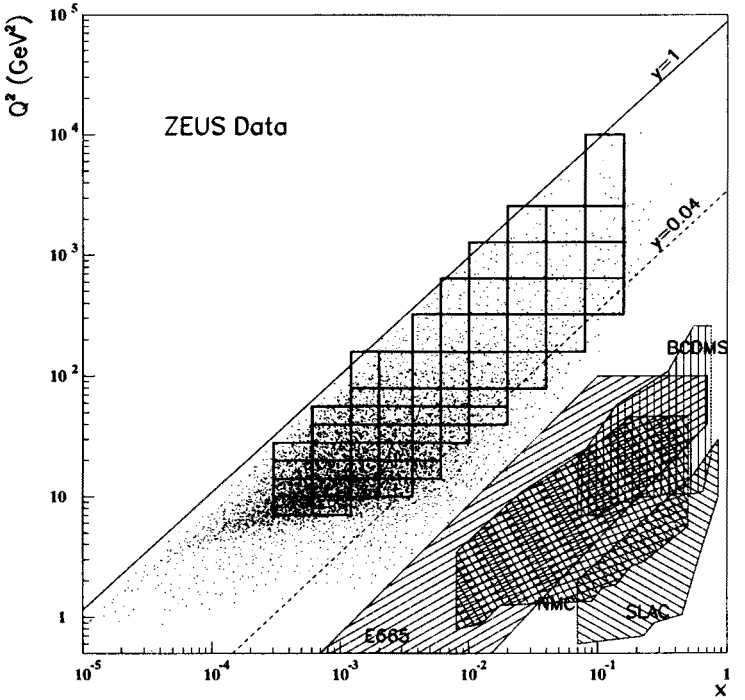

Fig. 1. The kinematical domains covered by the deep inelastic lepton nucleon scattering experiments

processes. In Chapter 2 I shall try to summarize what we have learned so far from the measurements of the proton structure function F_2 at HERA and discuss their QCD fit. The discussion of the hadronic energy flow as a function of the photon virtuality Q^2 is presented in Chapter 3. Finally, I shall discuss in Chapter 4 the diffractive processes giving rise to the "rapidity gap events". In particular I shall summarize what we have learned so far on the nature of the Pomeron.

2. The structure function F_2

2.1. Measurement of F_2

The proton structure function $F_2(x, Q^2)$ is determined from the measured inclusive differential cross section $d\sigma/dxdQ^2$. There are several important differences in the procedure and in the systematic accuracy of the differential cross section measured at HERA with respect to earlier measurements made by the fixed target experiments. The event kinematics is

reconstructed at HERA not only from the scattered electron angle and energy but also redundantly from the measured hadronic energy flow. This provides a valuable cross check of the systematic uncertainty of the measurement. The calorimetric measurement of the scattered electron energy give rise to worse resolution and larger energy scale error than in the fixed target experiments. In these experiments the outgoing electrons (muons) were measured in the magnetic spectrometers. On the other hand, owing to the colliding mode, the event topology at HERA can be more easily resolved. Note, that in the fixed target experiments all particles are emitted in a small size cone around the incoming lepton direction. One of the most important limitations of HERA experiments in extending the measurement domain towards higher $y = Q^2/sx$, where the exchange of longitudinally polarized photons largely contribute to the electron-proton scattering cross section, originates from a poor experimental means to control the background due to photo-production. On the other hand the radiative corrections, which for several fixed target experiments have to be unfolded from the experimental data, can be better controlled at HERA.

The structure function F_2 is derived from the measured differential cross section according to the following formula:

$$\frac{d\sigma^{ep}}{dxdQ^2} = \frac{2\pi\alpha^2}{xQ^4}(1+(1-y)^2)F_2^{ep}(x,Q^2))(1+\delta_{F_L}+\delta_{Z_o})(1+\delta_r)\,. \quad (3)$$

The corrections δ_{F_L} stands for the unmeasured fraction of the differential cross section due to photoabsorbtion of longitudinal photons. This correction has to be calculated using perturbative QCD. The corrections δ_{Z_0} reflects the contribution of the Z_0 exchange to the ep scattering (in the Q^2 domain discussed here mostly via the interference term). The corrections δ_r is the radiative correction dominated by the processes of the real photon emission by the incoming (outgoing) electron.

2.2. What can be concluded from the F_2 data

In Fig. 2 the structure function F_2 as measured at HERA is shown together with the data from the E665 [6], the NMC [7] and the BCDMS [8] experiments.

The data exhibit a strong rise of the F_2 with decreasing x. Such a rise was unexpected in a phenomenological model of [9]. The authors of the model expected a very slow increase of the structure function, similar to the increase of the total pp, πp, Kp and γp total cross section as a function of the center of mass energy s. Such a rise can be related, in the framework of the Regge model, to the exchange of the Pomeron trajectory between the scattered particles DL. On the other hand the observed rise of

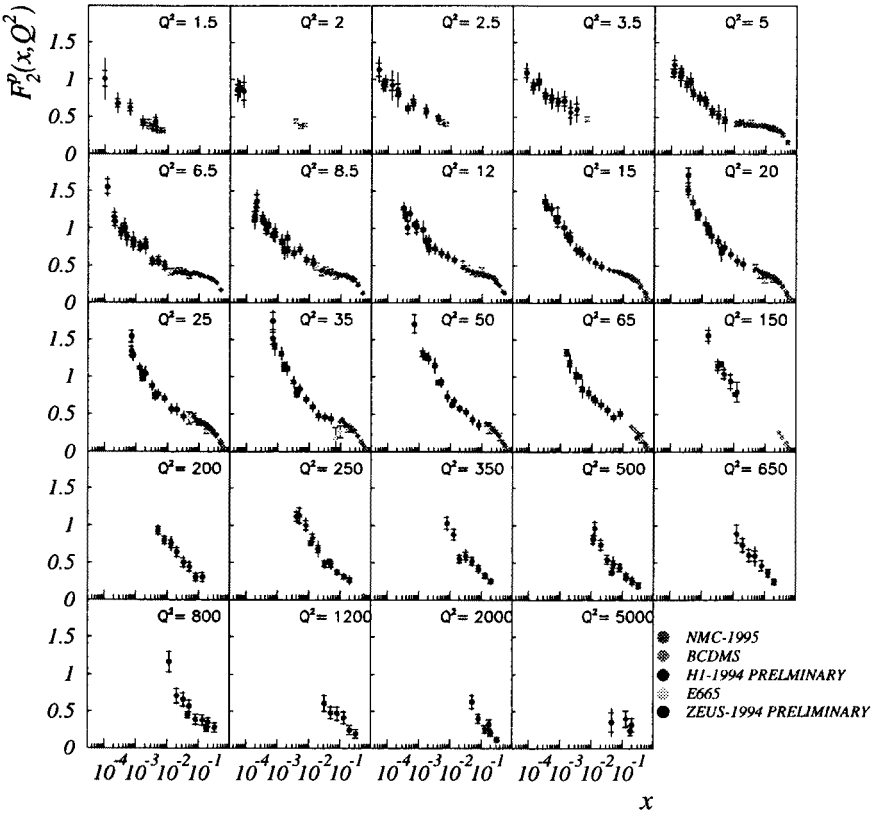

Fig. 2. The proton structure function $F_2(x, Q^2)$

F_2 in the low x region was predicted by a specific approximative solution of the BFKL equation (for more details see *e.g.* [10]). In addition, specific solutions of the DGLAP equations also predicted a fast rise of the F_2 in the low x region. In the approach of the authors of [11] the initial partonic distribution are specified at a very small virtuality scale $Q_0^2 = 0.34\,\mathrm{GeV}^2$. In such a case, even if no partons populate the low x region at this scale, they are "generated" by the DGLAP evolution equation giving rise to a large partonic density already at $Q^2 = 4\,\mathrm{GeV}^2$. In particular, a low x asymptotic solution of the DGLAP equation in which only singular part of the splitting functions was retained and in which only the evolution of the gluonic density is calculated [12] yield a strong rise of the F_2 in the low x region almost independently of the type of initial conditions.

2.3. What can not be constrained by the F_2 data

The form of the QCD prediction for the Q^2 evolution of F_2 leaves significant freedom in quantitative predictions. This is mostly due to the fact that neither the form of initial conditions for the evolution equations nor the domain of validity of the DGLAP and BFKL equation are fixed by the theory. Therefore, no firm answer can be given to the question: which evolution equation describes best the data in the low x region [13]. Similarly, one can not conclude if including higher order QCD corrections for the splitting and the coefficient functions calculated recently (see the talk of Martin at the Paris DIS95 workshop [14] for a summary of progress made recently in this domain) improve the quality of the QCD fit to the data. In addition, because of the large systematic errors and small Q^2 range covered at small x, we can neither confirm nor exclude a presence of the nonlinear shadowing terms introduced to the evolution equations in [15]. These terms are expected to play significant role for large density parton systems. As it has been shown in [16] they may modify the gluon distribution obtained from the standard QCD fits.

So far we have considered the electron proton scattering at high Q^2 where the perturbative QCD can be applied. What happens when the virtuality of the photon decreases such that the photon can be considered as a real particle? In order to compare these two regimes we define the cross section for the photoabsorbtion of virtual photons as:

$$\sigma_{\gamma^* p} = \frac{4\pi^2\alpha}{Q^2} F_2(W^2, Q^2), \tag{4}$$

where W^2 is the mass of the hadronic system ($W^2 \simeq Q^2/x$), and compare this cross section with the real photon cross section. The comparison is shown in Fig. 3. It is interesting to note that the cross section at $Q^2 = 2$ GeV^2 rises faster than the real photon (photo-production) cross section as a function of W^2 and at $Q^2 = 2$ GeV^2 and $W = 100$ GeV it reaches the value of about 40 % of the photo-production cross section. This means that the transition between the hard, controllable by perturbative QCD, and soft, non-controllable by perturbative QCD, processes is very smooth. The intriguing question is: how close can we approach the soft, photo-production domain, using the framework of perturbative QCD and how smooth is the transition? This and several other questions will be answered as new data are collected in the Q^2 domain between 10^{-2} and 1 GeV^2 for large W.

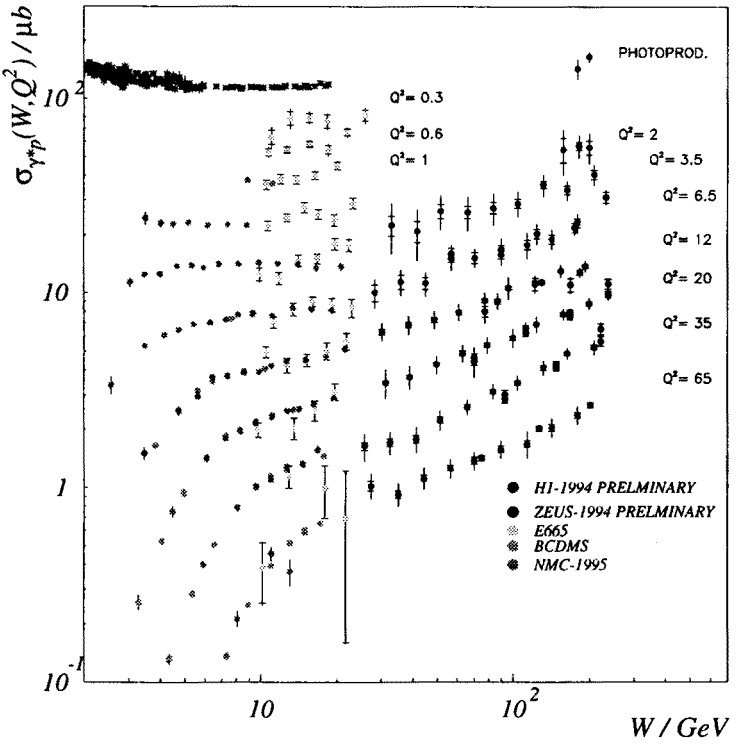

Fig. 3. The W dependence of the cross section for the photoabsorbtion of the real and virtual photons.

3. Hadronic energy flow

The surprising observation made as soon as the first HERA data were analyzed [17, 18] was the appearance of two distinct event classes corresponding to different energy flow in the detectors. In most of DIS events, such as the one shown in Fig. 4, hadrons are emitted in the angular range covering angles down to zero degrees with respect to the direction of the incoming proton. There exist however a significant fraction of events in which no hadrons are detected below an angle θ_0 which can be quite large as shown in Fig. 5.

These events have been named the "rapidity gap events". Their origin and characteristics will be discussed in Chapter 5. In this Chapter I shall discuss the hadronic flow for events in which no rapidity gap was observed. I shall focus in particular on the question: is there a significant difference in the topology of the hadrons produced in the processes involving large and

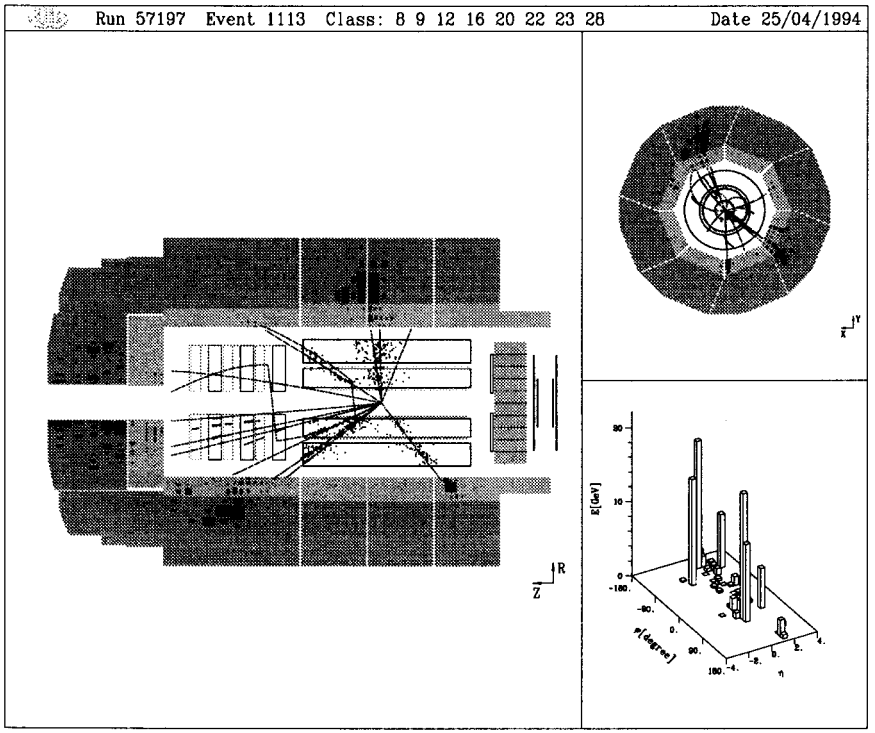

Fig. 4. A deep inelastic scattering event

small virtualities of the exchanged photon and what are the footprints of the high virtuality photon in the energy flow observed in the detector.

I shall discuss below the measurement of the hadronic transverse energy flow as a function of pseudo-rapidity $\eta^* = -\ln(\tan(\theta^*/2))$. We shall use here the center of mass reference system of the collision of the virtual photon with the proton. We define in this reference frame the transverse energy in the η^* bin as:

$$E_T(\eta^*) = \Sigma_\phi E_i \sin(\theta(\eta_i^*)) , \tag{5}$$

where, E_i is the energy deposited in the i-th calorimetric cell. The distributions $dE_T/d\eta^*$ normalized to the total number of events is shown in Fig. 6 as a function of the pseudo-rapidity.

In order to exclude the rapidity gap events it is required that the energy deposited up to the angle of 15 degrees is larger than 0.5 GeV. The acceptance region of the H1 detector is such that the energy flow in the fragmentation region of the photon (negative η^*) and the central region $\eta^* \simeq 0$

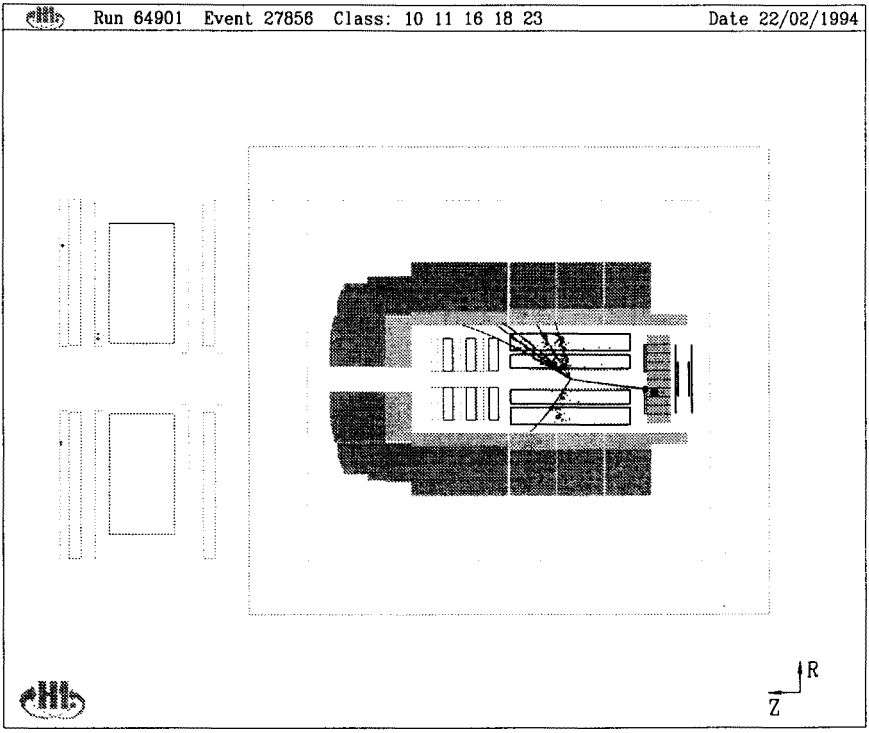

Fig. 5. A diffractive deep inelastic scattering event.

is measured (the $\eta^* = 1$ value corresponds to the detector boundary). The distributions correspond to 4 bins of the photon virtuality (transverse size of the interaction region) and the fixed region of y chosen to lie between 0.3 and 0.5. We observe Q^2 independent hadronic energy flow in the central region and, as expected for particles originating from fragmentation of small size objects, larger transverse energy flow in the photon fragmentation region for large Q^2 scattering. In Fig. 7 we focus on the Q^2 dependence of the energy flow in the photon fragmentation region and in the central region.

It is striking, that the transverse energy flow in the central region is independent of the virtuality of the photon. This means that large virtuality in the upper part of the diagram shown in Fig. 8, where the virtual photon couples to the quark, is diffused away very quickly while going down in the ladder such that the particle emission in the central region is independent of the transverse size of the interaction volume.

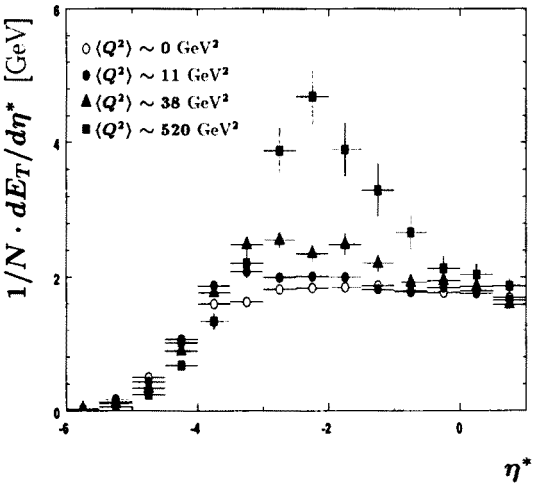

Fig. 6. The flow of the mean transverse energy in the CMS reference frame for DIS and photo-production events

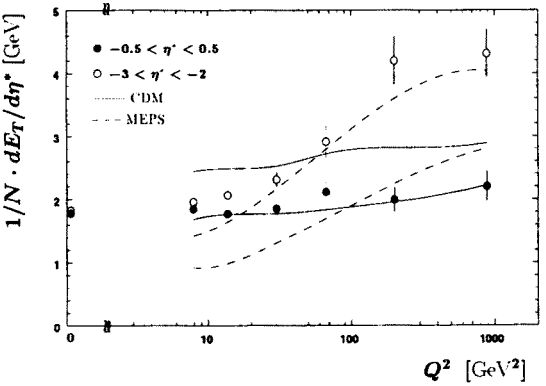

Fig. 7. The Q^2 dependence of the transverse energy per unit of pseudo-rapidity in the central region and in the photon fragmentation region.

As a consequence of this observation we can conclude that the contribution of events in which the large virtuality propagates down in the ladder and gives rise to a jet of transverse momentum of the order of Q is small and its contribution to the inclusive cross section can be neglected. In addition, we observe similar spectrum of E_T for the photo-production and for the DIS events up to large transverse energies as shown in Fig. 9a. It is even more striking that, in the photon fragmentation region, the virtual photon of $Q^2 = 10 - 20\ \mathrm{GeV}^2$ radiates similarly as a vector meson of much larger

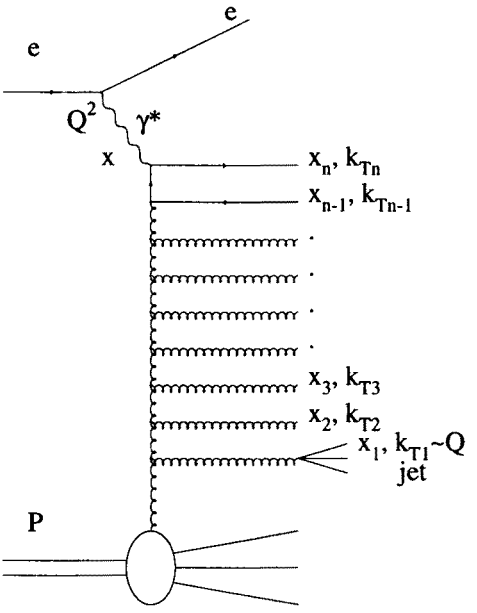

Fig. 8. The QCD diagram for DIS scattering

size. This simple feature of the data is badly described by the existing QCD based models shown in Fig. 7 [20, 21] indicating that the transition from the processes involving short distance interactions to soft (large distance) processes is, as far as the transverse energy flow is considered, more simple than expected by the QCD based models.

4. What is a Pomeron

As I have pointed out in previous Chapter there exist two distinct classes of events having different characteristics of the energy flow observed in the detectors. In the class of rapidity gap events no energy is deposited below a certain angle θ_0^* measured with respect to the incoming proton direction. In Fig. 9b the distribution of the $\eta^*_{\mathbf{max}} = -\ln(\tan(\theta_0^*/2))$ is shown. By definition the angle θ_0^* is the minimal angle in the photon-proton CM-system of the reconstructed track or the energy cluster having the momentum (energy) larger 400 MeV. The two distributions correspond to the interactions of quasi-real photons and to the deep inelastic scattering with the virtuality of the photon in the range 10–100 GeV^2. Both spectra peak at the pseudorapidity corresponding to the minimal angle of the detector acceptance in

the proton direction. The spectra are expected to fall exponentially for decreasing values of $\eta^*_{\max}$. The observed excess (plateau) at negative values of $\eta^*_{\max}$ indicates a presence of distinctly different mechanisms which produce these events. The striking feature of this plot is that the $\eta^*_{\max}$ spectra, when normalized to the total number of events, exhibit Q^2-independent shape and normalization despite quite different interaction mechanism. Let us try to find a simple qualitative explanation of this similarity. Let us assume that the incoming proton fluctuate into two color neutral systems and that the life time of such a fluctuation is larger than both:

- the typical time of a fluctuation of a real photon into the ρ meson $\tau \geq 2sy/M_p M_\rho^2$, where M_p is the proton mass and M_ρ is the ρ meson mass
- the typical interaction time of the virtual photon $\tau_{\rm DIS} \geq sy/M_p Q^2$.

In such a case the real (virtual proton) interacts either with a proton or, if it encounters a proton fluctuating into two color neural systems, it interacts with one of them such that its partner remains undisturbed. If the ratio of probabilities for interactions of real (virtual) photons on a proton (dissociated proton) are the same than similarity of the $\eta^*_{\max}$ spectra reflect the universal spectrum of the missing longitudinal momentum carried by the spectator system. The rapidity gap events with large negative $\eta^*_{\max}$ corresponding to a configuration in which the spectator system carries almost all the incoming proton momentum. The observed similarity can be qualitatively understood in analogy to the process of real photon radiation by the incoming electron in DIS processes. The shape of the spectrum of photons emitted at small angles (of the order of m_e/E_e, where m_e is the electron mass and E_e its energy) is independent of the Q^2 of the interaction leading to the universal, Q^2 independent, spectrum of the missing longitudinal momentum (in the direction of the incoming electron). The formation time of photons emitted at such small angles is much larger than the interaction time of the virtual photon with the proton giving rise to this universality. Following this analogy we can conclude that, in the rapidity gap events, the four-momentum transfer from the incoming proton to the spectator system is much smaller than both Q^2 and M_ρ^2.

Following the qualitative analysis let us discuss now the DIS rapidity gap events quantitatively. The measurements discussed below use two kinematical variables which have not been defined so far:

$$x_{\rm pom} = \frac{q(P-P')}{qP}, \tag{6}$$

$$\beta = \frac{Q^2}{2q(P-P')}, \tag{7}$$

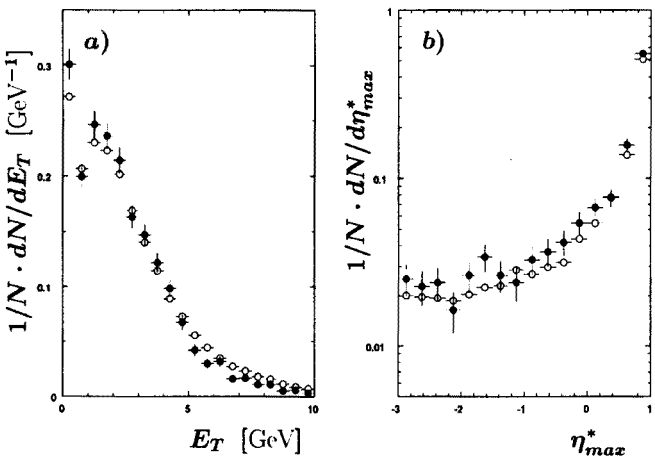

Fig. 9. The distribution of the transverse energy in the central region (a) and of the $\eta^*_{\max}$ (b) for the photoproduction (open circles) and DIS (full circles) data.

where P' represents the four-momentum of the spectator system. Within a qualitative picture outlined above the variable $x_{\mathbf{pom}}$ may be interpreted as the fraction of the 4-momentum of the incoming proton carried by the one of the two systems resulting from the proton dissociation - the one which interacts with the photon. For large Q^2 processes the quantity β can be interpreted as the momentum fraction of the interacting system carried by its charged parton. Note that $x = \beta x_{\mathbf{pom}}$. It should be stressed that this interpretation is valid for processes in which the momentum transfer squared $t = (P - P')^2$ is significantly smaller than both Q^2 and M_ρ^2.

We shall discuss below the physics implications of the measurement of the structure function $F_2^{D(3)}$ defined as:

$$\frac{d^3\sigma}{dx dQ^2 dx_{\mathbf{pom}}} = \frac{4\pi\alpha^2}{xQ^2}\left(1 - y + \frac{y^2}{2}\right) F_2^{D(3)}(x, Q^2, x_{\mathbf{pom}}) . \qquad (8)$$

This equation follows from formal differentiation of (3) over t and $x_{\mathbf{pom}}$, neglecting the contribution of longitudinal photons to the cross sections, and integrating the four-fold differential cross section over the t-range where the spectator system remains undetected in the main detector (for more details see *e.g.* [22]).

The structure function $F_2^{D(3)}$ is shown in Fig. 10 as a function of $x_{\mathbf{pom}}$ for several Q^2 and β bins. The striking feature of this plot is that it exhibits a universal behavior of $F_2^{D(3)}$ as a function of $x_{\mathbf{pom}}$. If the $F_2^{D(3)}$ is

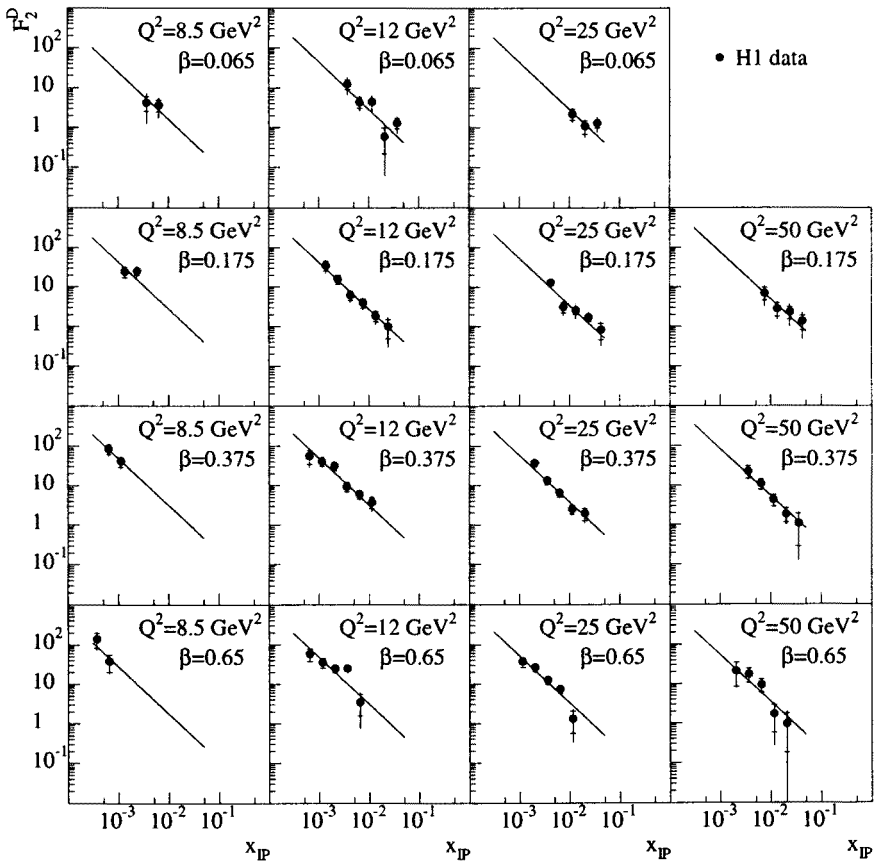

Fig. 10. The structure function $F_2^{D(3)}(Q^2, \beta, x_{\mathrm{pom}})$ as measured by the H1 collaboration.

parametrized as:

$$F_2^{D(3)}(Q^2, \beta, x_{\mathbf{pom}}) = A(Q^2, \beta) x_{\mathbf{pom}}^n , \tag{9}$$

than fits of good quality are obtained, yielding $n = 1.19 \pm 0.06(\mathrm{stat}) \pm 0.07(\mathrm{syst})$ [22] for H1 and $n = 1.30 \pm 0.08(\mathrm{stat}) + 0.08 - 0.14(\mathrm{syst})$ [23] for the ZEUS data (the recent preliminary value of the n presented by the ZEUS collaboration at the Beijing conference [24] is somewhat higher).

If high energy diffraction is the source of rapidity gap events than the exponent n specifying the $x_{\mathbf{pom}}$ dependence of the $F_2^{D(3)}$ can be expressed, within the Regge model, as $n = 2\overline{\alpha} - 1$. The $\overline{\alpha}$ parameter is related to the

high energy rise of the hadron-hadron cross section which was observed [25] to have an universal (independent of the hadron type) behavior: $\sigma_{\mathrm{tot}}^{h1,h2} \simeq s^{\overline{\alpha}}$ with $\overline{\alpha} = 1.08$ The processes having such a high energy asymptotic are classified as those originating from the Pomeron exchange. The apparent consistency between the measured values of n and $\overline{\alpha}$ value suggests that diffractive processes give rise to the rapidity gap events seen at HERA. Consequently, we shall consider the rapidity gap events as originating from interactions of the photon with the Pomeron carrying a fraction $x_{\mathbf{pom}}$ of the parent proton momentum. The Pomeron needs not to have properties of a particle *e.g.* it can be a part of the proton, it is however indispensable that the system is color neutral such that the rapidity gap is produced.

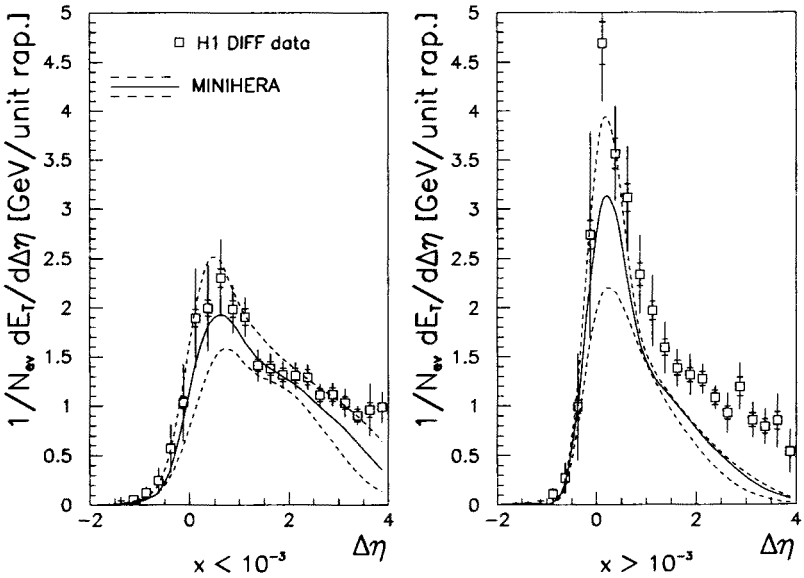

Fig. 11. The mean transverse energy flow for rapidity gap events compared to the simulations for electron proton scattering at reduced incoming proton energy.

What is the Pomeron? Let us first assume that it is a hadron-like object. In such a case the electron-Pomeron interaction should resemble the electron-proton interaction at the reduced center of mass energy which can be calculated from the $x_{\mathbf{pom}}$ value. In Fig. 11 the transverse energy flow is shown for rapidity gap events and compared with the Monte-Carlo calculation for the electron proton scattering. The energy of the proton corresponding to the average value of $x_{\mathbf{pom}}$ is 2.46 GeV. The energy flow calculated for such a proton energy is shown as the full line and the broken

lines correspond to the proton energies of 8.2 GeV and 0.82 GeV which reflect the available range of the $x_{\mathbf{pom}}$ values. What can be concluded from this plot is that, as far as the transverse energy flow is considered, the electron-Pomeron interactions resemble that of electron-proton interactions.

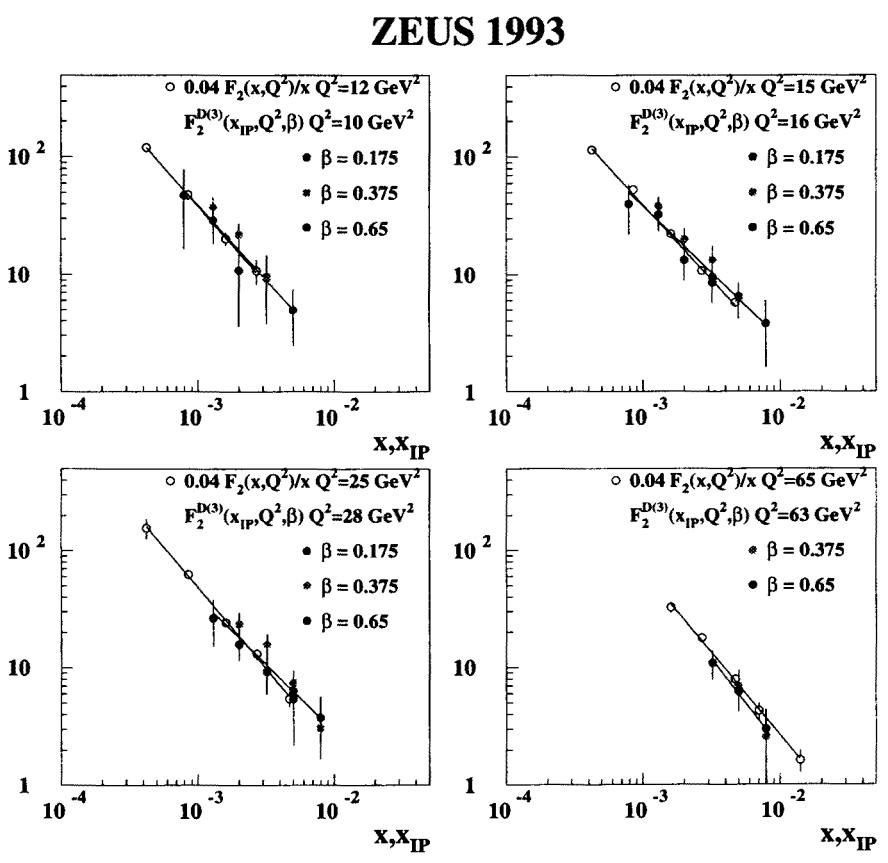

Fig. 12. A comparison of the diffractive and non-diffractive structure functions.

Another interesting observation is that the distribution of the momentum fraction of the proton carried by the Pomeron is, in the low x region, similar to the distribution of the momentum fraction of the proton carried by the gluon which is proportional to $x^{-1.22}$ at $Q^2 = 4$ GeV^2 The above exponent is compatible with the n values measured both by the H1 and ZEUS collaboration. This similarity is reflected in the similar shape of the F_2 and $F_2^{D(3)}$ shown in Fig. 12 as a function of x ($x_{\mathbf{pom}}$) for various values

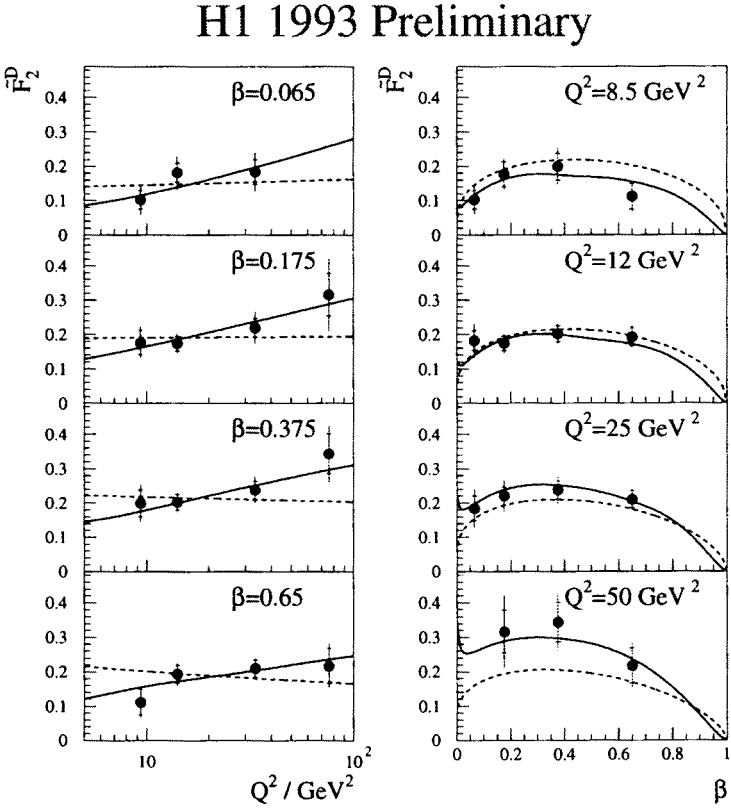

Fig. 13. The NLO fits to the $F_2^{D(3)}$ data.

of β. If the Pomereon were a gluon than the color field stretched between the proton and the gluon would fill in the gap with particles. Therefore, in such a picture an exchange of additional gluon is needed to neutralize the color transferred to the Pomeron. The similarity of the observed gluon and the Pomeron spectra imply that, if an additional gluon is exchanged, its momentum has to be much smaller than the momentum of the first one leading to effective factorization of the $F_2^{D(3)}$. Exchange of such small momentum gluon may be a large distance nonperturbative effect and in such a case its gluonic picture may breake down altogether.

The integral of the structure function $F_2^{3(D)}$ over $x_{\mathbf{pom}}$ is, assuming factorization, proportional to the Pomeron structure function $F_2^{\mathbf{pom}}(\beta, Q^2)$. The normalization of the function can not be unambiguously fixed as the normalization of the Pomeron flux is arbitrary. If the Pomeron has quarkonic

and gluonic structure which does not mix with that of the parent proton, we can check if the corresponding quark and gluon distributions in the Pomeron obey the characteristic pattern of the scaling violation predicted by perturbative QCD. The QCD fit of the structure function $F_2^{\mathbf{pom}}(\beta, Q^2)$ is shown in Fig. 13. The fit has been made using the same procedure as the one described in detail in Chapter 2. Two fits have been made. In the fist one, an assumption was made that at the $Q_0^2 = 4$ GeV^2, where the initial conditions for the evolution equations are specified, the Pomeron is composed only of quarks. The corresponding NLLO fit is shown in Fig. 13 as the dashed line. Better quality fit is obtained if one assumes that at Q_0^2 the Pomeron is composed both of quarks and gluons. Such a fit describes well the Pomeron structure function evolution. The shapes of the distribution of momenta carried by the gluons and quarks obtained as the fit result at $Q_0^2 = 4$ GeV^2 are shown in Fig. 14. As we could expect from the previous discussion the best QCD fit corresponds to a configuration in which almost all of the Pomeron momentum is carried by the gluon leaving very small momentum fraction to both the quarks and softer gluons.

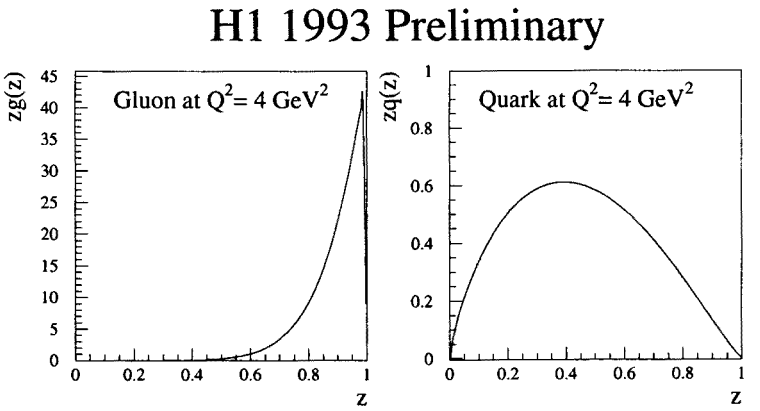

Fig. 14. The momentum density of gluons and quarks in the Pomeron at $Q^2 = 4$ GeV^2.

The internal structure of the Pomeron can be studied as well by measuring the jets produced in rapidity gap events. The ZEUS analysis [26] shows that, within a specific assumption concerning the shapes of the gluon and the quark distributions, the total momentum carried by gluons is between 36 and 70 %, independently of the value of the Pomeron flux factor.

5. Conclusions

The experiments at HERA are extending our understanding of strong interactions. Apart from classical large Q^2 processes, where perturbative QCD can be tested, a new "HERA-specific" research domain is emerging. Novel studies are focused on exploring the transition between the hard and the soft interactions, at small and large longitudinal distances, between point-like and extended hadronic objects. Progress in this domain is likely to be driven by experimental results and HERA may play an important role here.

REFERENCES

[1] R.P. Feynman, *Photon-Hadron Interactions*, W.A. Benjamin Co., New York 1972.
[2] J.D. Bjorken, *Phys. Rev.* **179**, 1547 (1969); J.D. Bjorken, A. Paschos, *Phys. Rev.* **185**, 1975 (1969).
[3] B.L. Ioffe, *Phys. Lett.* **30**, 123 (1969).
[4] H1 Collaboration, The H1 Detector ar HERA, DESY93-103 (1993).
[5] ZEUS Collaboration, The ZEUS detector, Status Report (1993).
[6] A.V. Kotwal *et al.*, Presented at the XXXth Rencontres de Moriond, March (1995), FERMILAB-Conf-95/046-EXP.
[7] P. Amaudruz *et al.*, *Phys. Lett.* **B295**, 159 (1992).
[8] A.C. Benvenutti *et al.*, *Phys. Lett.* **B223**, 485 (1989).
[9] A. Donnachie, P.V. Landshoff, M/C-th 93/11, DAMTP 93-23.
[10] J. Kwiecinski, Lectures given at the 23nd Schladmig Winter School, Report 1620/PH, IFJ Cracow (1993).
[11] M. Glück, E. Reya, A.Vogt, *Z. Phys.* **C53**, 127 (1992); M. Glück, E. Reya, A.Vogt, *Phys. Lett.* **B306**, 391 (1993).
[12] A. De Rujula *et al.*, *Phys. Rev.* **D40**, 1649 (1974).
[13] H1 Collaboration, Nucl. Phys. **B449** (1995) 3.
[14] A. Martin, Talk given at the DIS95 workshop, Paris, April 1995, to appear in the workshop proceedings.
[15] V.N Gribov, E.M. Levin, M.G. Ryskin, *Sov. J. Nucl. Phys.* **15**, 438, 675 (1972).
[16] K. Golec-Biernat, M.W. Krasny, S. Riess, *Phys. Lett.* **B337**, 367 (1994).
[17] ZEUS Collaboration, M. Derrick *et al.*, *Phys. Lett.* **B315**, 481 (1993).
[18] H1 Collaboration, T. Ahmed *et al.*, *Nucl. Phys.* **B429**, 477 (1994).
[19] H1 Collaboration, S. Aid *et al.*, *Phys. Lett.* **B358**, 412 (1995).
[20] L. Lonnblad, *Comput. Phys. Commun.* **71**, 15 (1992).
[21] G. Ingelman, Proc. HERA workshop, Hamburg 1991, Vol3 1366.
[22] H1 Collaboration, S. Aid *et al.*, *Phys. Lett.* **B348**, 681 (1995).
[23] ZEUS Collaboration, M. Derrick *et al.*, DESY 95-093 (May 1995).

[24] ZEUS Collaboration; M. Derrick *et al.*, Cross Section Measurement of Diffractive Production in Deep Inelastic Scattering, Contribution for Beijing Conference August 1995, China.
[25] A. Donnachie, P.V. Landshoff, *Phys. Lett.* **B296**, 227 (1992).
[26] ZEUS Collaboration, M.Derrick *et al.*, *Phys. Lett.* **B356**, 129 (1995).